International Journal of Innovative Computing, Information and Control
Volume **18**, Number **4**, August **2022**

ICIC International ©2022 ISSN 1349-4198
pp. **1217–1234**

COMPUTER-AIDED TRANSMITTED DEFORMATION INSPECTION SYSTEM FOR SEE-THROUGH GLASS PRODUCTS

Hong-Dar Lin[1,*], Yuan-Chin Lo[1] and Chou-Hsien Lin[2]

[1]Department of Industrial Engineering and Management
Chaoyang University of Technology
No. 168, Jifong East Road, Wufong District, Taichung 41349, Taiwan
s10215616@cyut.edu.tw
*Corresponding author: hdlin@cyut.edu.tw

[2]Department of Civil, Architectural, and Environmental Engineering
The University of Texas at Austin
301, East Dean Keeton Street, Austin, Texas 78712-0273, USA
chslin@utexas.edu

Received November 2021; revised March 2022

Abstract. *A vehicle windshield with deformation flaws will likely distort the driver's view of surrounding objects, leading to errors in visual judgment that may be dangerous to other road users. Since imaging deformations directly affect the quality of the see-through glass products, the measure and control of such deformations are crucial for industrial manufacturers. This study proposes an alternative to human evaluators in the process through developing a frequency reconstruction method established on computer vision to automatically detect deformation flaws in transparent glass products. To quantify the deformation level of a curved glass product, we exploit the digital imaging of a known standard pattern with regular elements through a testing sample to capture a transmitted deformation image of that sample. Then, the proposed method applies the Hough transform voting scheme to finding the peak points of the base elements in parameter space, and reconstructs the base elements of the captured image by the inverse Hough transform. The binary testing image subtracts the binary reconstructed image to obtain a binary difference image displaying the detected deformations. Experimental outcomes present the proposed approach using grids pattern reaches a high 83.85% probability of exactly discriminating deformation flaws on transmitted appearances of transpicuous glass.*
Keywords: Transpicuous glass product, Transmitted imaging, Imaging deformation, Optical inspection, Hough transform voting scheme

1. **Introduction.** Transparency in materials allows light to travel through them unaffected, thus making the materials see-through. Transparent materials are used in the production of many commercial products, such as clear substrates, polarizing film, diffusers, optical fibers, plastics, and glass. Since imaging deformations directly affect the quality of the see-through glass products, the measure and control of these deformations are crucial for industrial manufacturers. Such deformations may occur when the object is subjected to mechanical or thermal loads.

In the vehicle windshield production process, deformation flaws may form on the windshield if the furnace temperature is not properly controlled during the baking procedure. Deformation flaws in the windshield will distort the driver's perception of the shape and motion of nearby objects, causing visual misjudgments that may be dangerous to other

DOI: 10.24507/ijicic.18.04.1217

road users. Compared to regular plane glass, outwardly curved glass usually exhibits higher transmission, higher reflectance, and wider field of view. Currently, outwardly curved glass is widely used in vehicle windscreens, rearview mirrors, and security mirrors to provide drivers with better fields of vision on the road. Since the transmitted deformation flaws directly affect the imaging quality of vehicle glass, the detection of the kinds of flaws is very important for car windshield manufacturers.

Transmitted deformation regularly has existence in vehicle glass to a certain level because of the glass curvature. Figure 1 shows two transmitted deformation scenes through defective car windscreens. The transmitted shapes of objects in the images are significantly distorted; deformation flaws in the windscreen make the transmitted objects appear irregular, out of focus, or blurry to the driver. These distortions may contribute to driver errors and lead to dangerous accidents.

FIGURE 1. Two transmitted deformation scenes through defective car windscreens

Inspection of deformation flaws during the manufacturing process has its own set of difficulties. Deformation flaws influence as well the imaging quality of industrial glass products as their performance, features and aesthetics. Currently, the most common methods for detecting deformation flaws in the industry rely on human visual inspections. Human inspection is prone to errors due to the inspectors' subjectivity, especially when the eyes are fatigued. Figure 2 shows a typical human inspection task, including a windscreen sample, a windscreen support frame, and an inspector measuring transmitted deformations in the imaging area of a standard pattern, and testing the sample by hand with a sliding caliper. Figure 3 illustrates three standard pattern shapes commonly used in human visual inspection: straight lines shape, grids shape, and checkerboard shape. Furthermore, difficulties

(a) (b) (c) (d)

FIGURE 2. (a) A windscreen sample; (b) a windscreen support frame; (c) and (d) an inspector measuring transmitted deformations in the imaging area of a standard pattern through a windscreen by hand with a sliding caliper

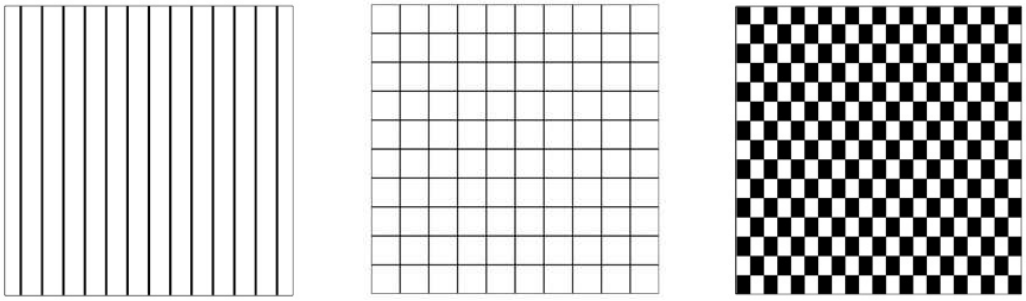

(a) (b) (c)

FIGURE 3. Three standard pattern shapes commonly used in human visual inspection: (a) Straight lines shape; (b) grids shape; and (c) checkerboard shape

also exist in accurately evaluating deformation flaws by computer-aided optical inspection systems since when imaging images are being acquired, the regions of deformation faults would enlarge, lessen or surprisingly pass from sight due to unbalanced lighting of the surroundings, distinct view angles of the evaluators, forms of transmitted patterns, and a variety of other factors.

The practical computer-aided vision system worked with the offline and sampling strategy uses a standard pattern imaged on glass to capture images and measure deformation magnitudes by hands with gauges. The high transmission and reflectance of glass samples often hinder the ability of current optical systems to precisely inspect glass deformation flaws. The properties of higher transmission and reflection on curved outward glass increase the difficulty of discrimination of the deformation flaws on vehicle glass products. This study presents the design of an automated distortion flaw detection system for transparent glass and proposes a Hough transform (HT) based approach to distinguish transmitted deformation flaws on curved car glass.

The HT is an efficient skill for isolating features of a specific shape in an image. It converts an object detection question in the image domain into a simpler local peak detection issue in the parameter domain [1]. The use of HT is suggested for having gap tolerance in feature border representations and is comparatively uninfluenced by image noise. The HT has superior capabilities for handling the cases of partially deformed and noisy shapes due to its voting scheme. Encouraged by these excellent properties, this study proposes the method of applying the HT voting scheme to finding the peak points of the base elements in parameter space, and reconstructs the base elements of the captured image by the inverse HT for finding the deformation flaws. The proposed approach, based on computer vision, can substitute for human inspectors in the traditional deformation inspection tasks during transparent glass production.

The rest of the article is composed as follows. Firstly, we review the articles on current techniques of computer vision for deformation flaw inspection. Secondly, we describe the proposed image procedures for detecting deformation flaws in transparent glass products. Thirdly, we execute the trials and assess the manifestation of the suggested model with a traditional technique. Finally, we conclude the contributions and indicate the further directions.

2. **Automated Defect Inspections.** Automatic optical inspection (AOI) in quality evaluation has become an essential process for production as it ensures that product quality is assured and production efficiency is enhanced through strict inspection and

testing of all products in the manufacturing processes [2-6]. The AOI systems based on image processing and machine learning techniques have generated many applications in the manufacturing industry, such as examination of holes on printed circuit boards [7], surface defect inspection in crucial parts of the high-speed trains [8], detection of appearance defects under unbalanced lighting condition using four real-world defect datasets [9], evaluation of slate slabs with regard to visual quality for construction purpose [10], and classification of steel exterior defects [11]. Surface quality inspection based on optical technology satisfies the quick and precision needs of a fabrication line and has been widely utilized in various industrial areas [2-4,6,12].

To improve glass product qualities, many studies have been developing non-contact automatic inspection devices inspecting the shape and poor surface of a glass product with the latest and image processing technologies, analyzing the characteristics of glass. These researches investigated the surface defect inspection of glass-related products, such as developing a defect tracking system for optical thin film products in smart-display-device industry [13], implementing an inspection system for surface defects of car bodies [14], proposing a multi-crisscross filtering method established on Fourier domain to inspect surface defects of capacitive touch panels [15], applying the Hotelling's T2 statistic and grey clustering methods to cosine transform for detection of visible defects in appearances of LED lenses [16], and designing a visual inspection system for non-spherical lens modules of semiconductor sensors [17]. These optical inspection systems focus mainly on the surface flaw detection on glass related products.

Image distortions because of perspective have to be corrected to permit further image processing. Regarding the distortion detection and correction techniques, Mantel et al. [18] proposed two methods for determining the perspective distortion on electroluminescence images of photovoltaic panels, and Cutolo et al. [19] presented a quick method to calibrate transparent head-mounted panels making the use of a calibrated camera. It is evident that most of the distortion related works due to perspective concentrate on the distortion correction of optical lenses.

Transmitted deformation is the image degeneration of a visible object incurred by a transpicuous material. In inspection studies of transmitted deformation in industrial parts, Gerton et al. [20] investigated deformation patterns of Ronchi grids mathematically for determining the effects of distortions in eyewear products. Youngquist et al. [21] presented a novel explanation of optical deformation and permitted the use of a phase-shifting interferometer for determining the distortion of a large optical window. Dixon et al. [22] developed a system using the digital imaging and a classifier based on decision trees for quantifying optical deformation in aircraft transparencies. Lin and Hsieh [23] designed a vision system with a trapezoidal mask for image acquisition and applied slight deviation control techniques to inspecting distortion defects on curved car mirrors.

Currently, the majority of AOI systems of glass products mainly detect surface flaws and the deformation blemishes are not included. It is hard to accurately detect transmitted deformation flaws embedded on surface of curved glass of vehicles with the properties of higher transmission and reflection. Presently, very few research studies apply automated visual detection systems to detecting glass deformation flaws. Therefore, we propose a vision system based on Hough transform techniques to inspect transmitted deformation flaws on see-through glass products.

Hough transform, initially proposed by Hough [24] in 1962, can detect lines, circles and other structures if their parametric equations are known. It is a good way to improve image form detection when the form can be parameterized by a set of parameters in an equation [25]. The major merit of the HT skill is that it has gap tolerance in feature border representations and is comparatively uninfluenced by image noise. This can be

very helpful when trying to discover lines with small interruptions in them due to image noise, or when searching objects are partly blocked [26]. Related studies used HT based shape detections and its derivatives in defect inspections, such as detecting the little-contrast mura defects in uneven lighting images of liquid crystal display panels [27], using the adaptive thresholding, canny detector to take out edges and HT to locate the linear weld defects in noisy background [28], presenting a superior HT method to inspect surface defects of products with central symmetry distribution patterns having similarity between object and background [29]. Some works proposed hybrid approaches based on HT for defect detections and classifications, such as combining with the deep learning technique to achieve quick product inspection of bottled wine [30], fusing with the support vector machine classifier to inspect loosened bolts in civil structures with more bolt connection [31].

Most of the distortion related works focus on the distortion correction of optical lenses. Many of the automated inspection systems of glass and mirrors mainly detect surface defects and the distortion flaws are not included. It is difficult to precisely detect reflected distortion flaws embedded on surface of curved car mirrors with high reflection [23]. Currently, there is very little literature on inspection of transmitted distortion flaws on transpicuous glass using automated visual inspection system. This study develops an HT based vision system to inspect transmitted distortion flaws on curved car glass. Not only the serious deformation faults but also the minor flaws can be identified by the proposed method under proper parameter selection.

3. **Proposed Methods.**

This study proposes a vision-based system with a known standard pattern for image acquisition and applies HT voting scheme to inspecting deformation flaws on curved vehicle windscreen glass. Five stages are developed to perform the process of deformation flaw inspection. First, to quantify the deformation level of a curved vehicle glass, we apply the digital imaging of the standard pattern through a testing windscreen to creating a transmitted deformation map of that windscreen. This deformation map is regarded as a testing image to be analyzed to find the existence of deformations and locations of the flaws. Second, the testing image is transformed to Hough space to obtain the coordinates of the correct axis positions of the multiple base elements. Third, through the accumulator's voting technique to find the peak points of the base elements in Hough domain, an image with new base elements is reconstructed from the selected peak points by taking the inverse HT. Fourth, the binary testing image subtracts the binary reconstructed image to obtain a binary difference image displaying the detected deformation flaws. Fifth, three common standard patterns are used to detect deformation regions by the proposed approach for differentiating effects of deformation flaw inspection.

3.1. **Image acquisition.**

In this study, testing samples with length 25.4 cm, width 20.4 cm, and thickness 0.2 cm, are randomly selected from the fabrication line of a vehicle glass manufacturer. To clearly acquire images with digital imaging of a standard pattern through a testing sample for creating a transmitted deformation map of the sample, this study proposes a vision system with a standard pattern for image capture shown in Figure 4. Figure 4 explains the diagrammatic drawings (the front, top and side views) and the apparatus arrangement of image acquisition for capturing a testing glass. The testing sample is inserted in a custom-made fixture vertically and is located in front of the standard pattern. The testing sample is partitioned into 4 regions for individual image acquisitions. The standard pattern with base checkers is attached on a wall. A CCD (charge coupled device) camera with stand is used to take images from the view

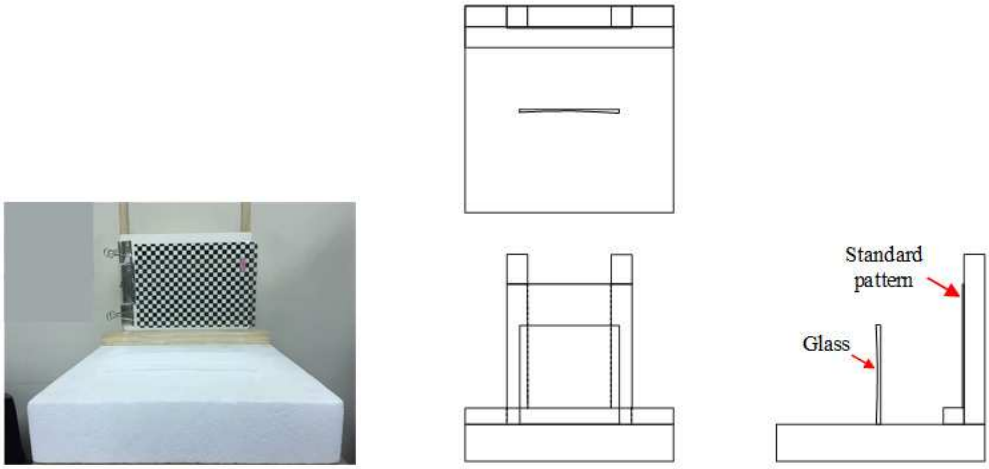

(a) (b)

FIGURE 4. The proposed vision system using the checkers pattern for image acquisition: (a) The front view from a CCD camera fixed on a stand, (b) the three perspective views of a testing glass sample inserted in a fixture and in front of a standard pattern

transmitted on the standard pattern through the testing glass. To acquire the digital imaging of a standard pattern with proper intensity, the lighting control of environment is also important when acquiring images.

3.2. **Image pre-processing.** For capturing better image resolution and representation of flaw evaluation, a trial specimen is partitioned into 4 parts for image capture. The captured image is pre-processed in several steps to increase the clearness of object appearances on transpicuous glass. Figure 5 shows the original testing image and enhanced image using two standard patterns performing the histogram equalization approach [32] for increasing contrast in gray levels. From the analysis of two corresponding intensity histograms, the contrasts of gray levels have been increased and the grids pattern and checkers pattern looked clearer in the enhanced images. To quantify the deformation level of the pattern image, Figure 6 depicts the binary edge images of the defective areas and normal regions that the Canny edge detector [33] and Otsu method [34] are applied to doing edge detection and segmentation sequentially while using the two standard patterns. Most of the base grids are clearly segmented from background in the binary images by the two methods. The results disclose that the slight deformation faults in transpicuous glass

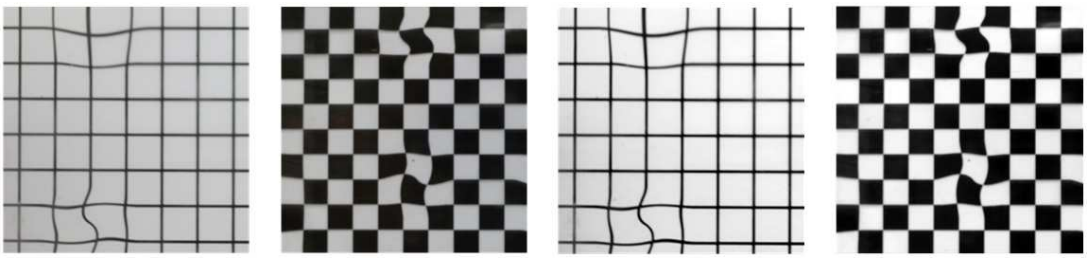

(a1) (b1) (a1-1) (b1-1)

FIGURE 5. The transmitted deformation images from digital imaging of the two standard patterns through testing defective windscreens: the captured images ((a1) and (b1)), the enhanced images ((a1-1) and (b1-1))

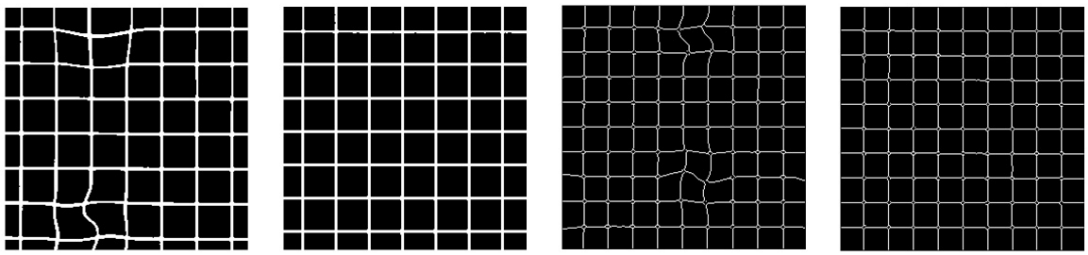

(a1) (a2) (b1) (b2)

FIGURE 6. The binary edge images ((a1) and (b1)) of defective areas and the corresponding images ((a2) and (b2)) of normal regions for using the two standard patterns

surfaces are rightly divided in the binary images, irrespective of insignificant deformation differences.

3.3. **Reconstruction of base element image by HT voting scheme.** The algorithm of HT can discover incomplete examples of objects inside some categories of shapes through a voting procedure. The motive of the HT is to fulfill clustering of boundary points into object potentials by conducting a clear voting process upon a group of parameterized image objects [24-26].

3.3.1. *Hough transform.* Straight line detection in binary images is a typical example by applying HT. The edge detectors are used as a preprocessing phase to gain boundary points that are on the wanted bend in the spatial domain. Owing to incompleteness in either the boundary pixels or the edge detectors, there perhaps have been losing pixels on the wanted bends and spatial variations between the perfect line forms and the noisy border pixels when they are gained from the edge detectors. For these causes, it is frequently a delicate matter to gather the extracted edge attributes to a suitable group of lines.

The common general form of a straight line equation is $y = ax + b$. This equation could be expressed as a pixel point (a, b) in the parameter domain. However, vertical lines would go up to boundless values of the slope parameter a. Therefore, for calculating causes, the Hesse polar form is proposed of employing the parametric expression of a line:

$$x \cos\theta + y \sin\theta = \rho \tag{1}$$

where variables θ and ρ are the angle between this vector and the x-axis, and the length from the origin to the line along a vector vertical to the line, respectively. Each point in the (x, y) plane gives a sinusoid in the (ρ, θ) plane. M collinear points lying on the line (Equation (1)) will give M curves that intersect at (ρ_i, θ_j) in the parameter plane. The HT creates a parameter domain matrix whose rows and columns correlate with these corresponding ρ and θ values. The linear HT arithmetic employs an accumulator, a two-dimensional array, to discover the presence of a line. The dimensionality of the accumulator is equivalent to the amount of not known parameters, i.e., two values in the pair (ρ, θ). The input to an HT is normally a binary image that has been segmented. We cannot find any significant visual difference between the normal and defective images in these Hough parameter domains.

3.3.2. *Accumulators and voting procedure in Hough domain.* Every component of the matrix is with a value equivalent to the amount of the pixels located on the line expressed by measurable parameters $H(\rho, \theta)$. In this way, the component having the largest value denotes the direct line which is highly representative in the original image. For every point

at $f(x, y)$ and its neighborhood, the HT arithmetic decides if there exists adequate proof of a straight line at that point. In this situation, we could compute the line parameters $H(\rho, \theta)$, and next seek the accumulator's bin which the parameters drop into, as well as cause a discrete increase in the value of that bin. The local maxima of the accumulators will give the significant lines. Figure 7 shows the relationship diagram between the binary edge image in spatial space and the corresponding accumulators in Hough parameter domain. It indicates that the standard pattern with 7 horizontal and vertical line segments is displayed on the binary image of a testing sample and there are 14 corresponding intersection points of curves in the Hough parameter space. The 7 horizontal and vertical line segments are the targets that need to be detected and their positions are located between the coordinates $H(107, 0°)$ and $H(362, 0°)$ for the horizontal line segments, and the coordinates $H(362, 91°)$ and $H(617, 91°)$ for the vertical line segments in Hough parameter domain.

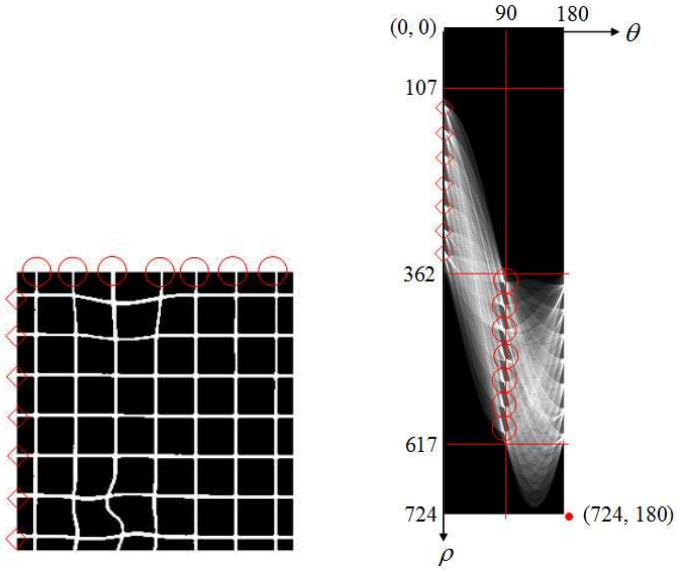

FIGURE 7. The relationship diagram between the binary edge image in spatial space and the corresponding accumulators in Hough parameter domain

By discovering the bins having the largest values, usually by seeking for local maxima in the accumulator's domain, the highly probable lines could be found. The straightforward means of discovering these peaks is via employing certain type of threshold. Because the lines went back do not include any length details, it is frequently needed to discover which parts of the image correspond to with which lines. In addition, owing to unideal variations in the edge detection procedure, there would generally be deviations in the accumulator domain, which might cause it complicated to discover the suitable peaks, and hence the adequate lines. Figure 8 shows the accumulators of the vertical and horizontal line segments for the dots pattern and checkers pattern in Hough parameter domains. For the grids pattern, Figures 8(a) and 8(b) indicate that there are 7 peaks in the accumulators of coordinates $H(362, 90°)$ to $H(617, 90°)$ and 7 peaks in the accumulators of coordinates $H(107, 0°)$ to $H(362, 0°)$ in Hough parameter domain. These two 7 peaks represent 7 vertical and 7 horizontal line segments in the spatial domain, respectively. Similarly, Figures 8(c) and 8(d) show two 9 peaks are found in the accumulators, representing 9 vertical and 9 horizontal line segments for the checkers pattern in spatial domain.

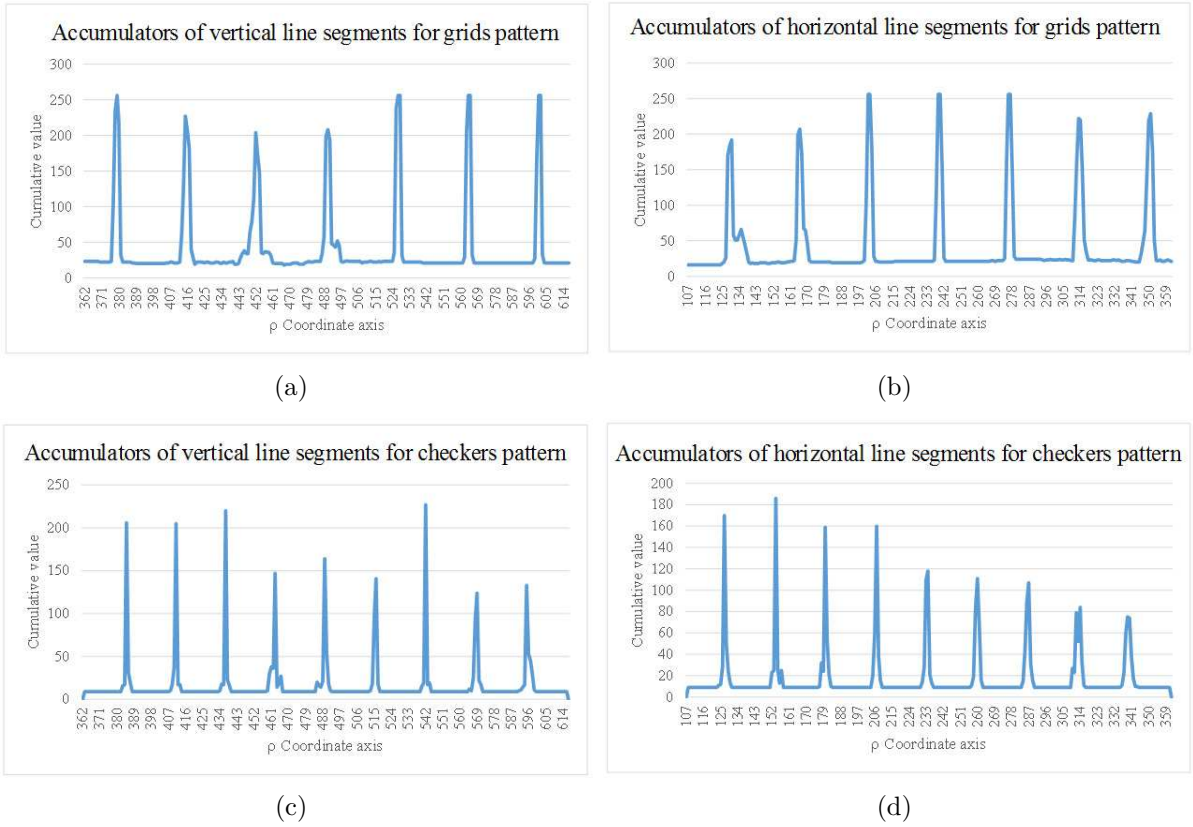

FIGURE 8. The accumulators of the vertical and horizontal line segments for the grids pattern ((a) and (b)) and checkers pattern ((c) and (d)) in Hough parameter domains

The HT generates parameter values ρ and θ for all lines that could go through each detected (by a threshold, in this example) image point. Each possible line through each point then votes for its ρ and θ values in a parameter space of possible ρ and θ values. We limit and quantize this parameter space to get an accumulator space which accumulates votes for ρ and θ values. After all possible lines through all detected points have voted, the accumulator space is searched for peaks that indicate which pairs of ρ and θ parameters got the most votes. A peak indicates the presence of line and gives its parameters and equation in the image. For the vertical line segments, let the ρ_i be the location of peak i in the parameter space, d is the distance between two line segments, x_0 is the initial location of the first vertical line segment in spatial domain. The location of peak i can be determined as follows:

$$\rho_i = Max\left\{H\left[x_0 + ((i-1)d), 90^\circ\right] \sim H\left[x_0 + (i \times d), 90^\circ\right]\right\} \tag{2}$$

3.3.3. *Reconstructed base element images.* After the positions of all peaks are located in parameter space, we need to transform them back to spatial domain for obtaining a base-line image. We assume $x_{i,k}$ be the coordinate of the i-th vertical line segment with the k-th peak for the image reconstruction in the spatial domain. It can be obtained as follows:

$$x_{i,k} = \rho_i - (\rho_1 - 1) \tag{3}$$

where the $\rho_1 = 362$ (i.e., $256 \times \sqrt{2}$) for image with size 256×256. The peaks in parameter domain transformed back to spatial domain are the vertical baselines in the reconstructed image. Similarly, the horizontal line segments follow the same voting procedure in Hough

domain and take inverse transform to obtain the horizontal baselines in the reconstructed image. Figure 9 shows the reconstructed images from the Hough domain for the grids pattern and checkers pattern images. The width of the vertical and horizontal baselines for the grids pattern is 4 pixels in Figure 9(a) and that for the checkers pattern is 1 pixel in Figure 9(b). These grids of the base-line image for the checkers pattern need to be further filled to become black and white checkers shown in Figure 9(b). These reconstructed images will be the binary base element images for comparing with those of the testing images to locate deformation flaws.

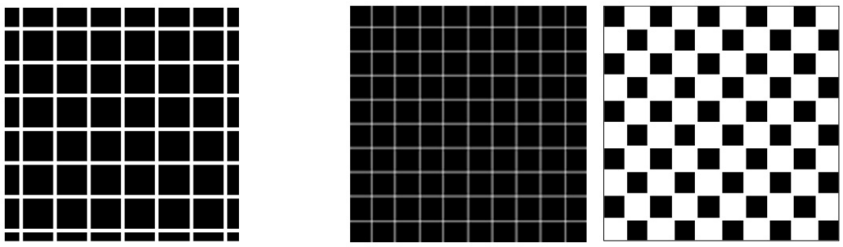

(a) (b)

FIGURE 9. The reconstructed images from the Hough domains of using (a) grids pattern, and (b) checkers pattern

3.4. **Binary difference images displaying the detected deformation.** If the binary testing image and the reconstructed base element image are precisely aligned, the deformation flaws can be identified and located through image subtraction. The binary testing image subtracts the binary reconstructed image to obtain a binary difference image indicating the locations of detected deformation flaws. The cumulative deviation ratios of deformed segments are calculated and the offset pixel ratio of deformed segments reveals the level of deformation in the image. Figure 10 shows the resulting binary images for the grids pattern and checkers pattern images.

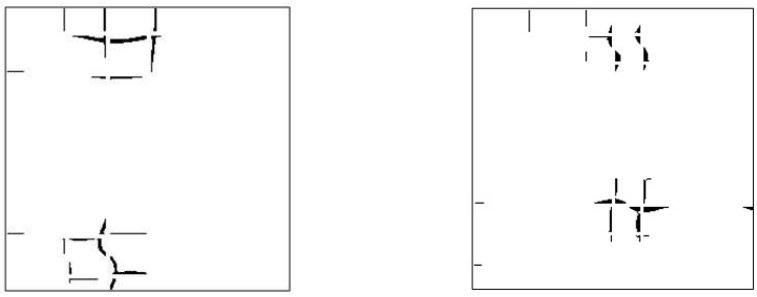

(a) (b)

FIGURE 10. The resulting binary images of using (a) grids pattern, and (b) checkers pattern

4. **Experiments and Results.** To assess performance of the suggested approach with three common standard patterns, assessments are performed on 80 real vehicle glass products (40 faultless samples without any flaws and 40 faulty samples with various transmitted deformation flaws) to evaluate the capability of the recommended technique. Every captured image including a quarter of a vehicle glass is with 256×256 pixels and each

pixel has 8 bits. The developed deformation flaw inspection arithmetic is compiled in Matlab platform and carried out on the version 7.9 of MATLAB interactive environment on a desktop computer (INTEL CORE i5-3230M 3.2GHz 8GB RAM).

To numerically verify the capability of the deformation flaw inspection methods, we discern the results of our assessments from those provided by the empirical evaluators (gold standard). Two indicators, $(1-\alpha)$ and $(1-\beta)$, are employed to indicate suitable detection appraisals; the greater the two indicators, the more accurate the detection consequences. Fake alert error α, considering regular regions as deformation flaws, divides the districts of regular regions inspected as deformation flaws by the districts of true regular regions to acquire the error. Losing alert error β, defeating to alert true deformation flaws, divides the districts of undetected true deformation flaws by the districts of overall true deformation flaws to gain the error.

4.1. **Successful rates for reconstructing base element images with various interval sizes among accumulators in Hough domain.** The interval size among accumulators in HT parameter domain will affect the success of producing a reconstructed image containing the whole base elements. An unsuitable interval among accumulators will result in producing a reconstructed image with incomplete base elements. Figures

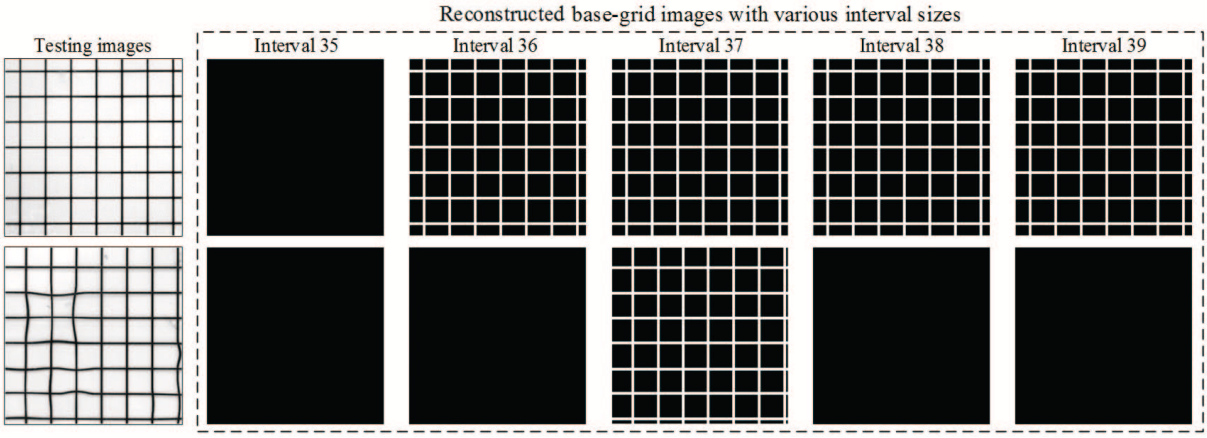

FIGURE 11. The initial images and corresponding reconstructed base-grid images with various interval sizes among accumulators in HT parameter domain

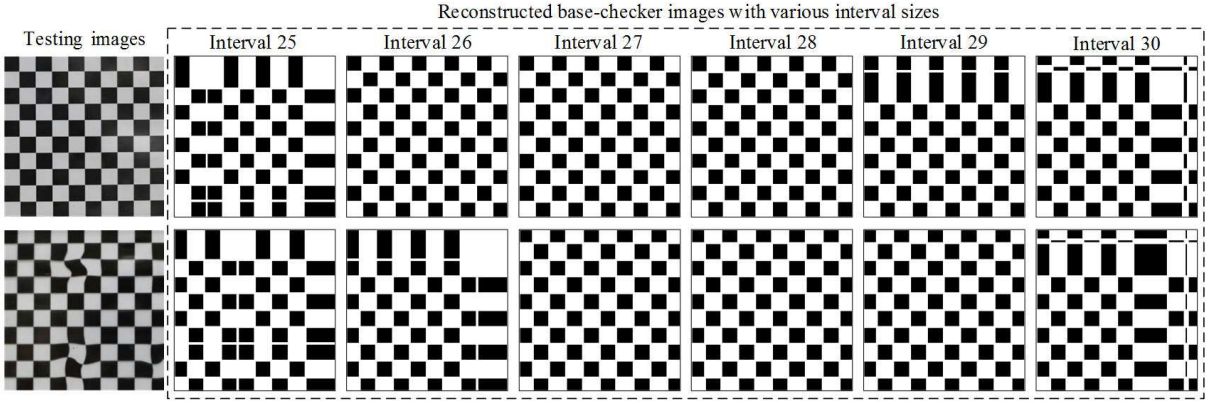

FIGURE 12. The initial images and corresponding reconstructed base-checker images with various interval sizes among accumulators in HT parameter domain

TABLE 1. The success rates of producing reconstructed base-grid images with various interval sizes among accumulators in HT parameter domain

Interval sizes	35	36	37	38	39
Failure number	24	1	0	13	13
Success number	305	328	329	316	316
Success rate	92.71%	99.70%	100%	96.04%	96.04%

TABLE 2. The success rates of producing reconstructed base-checker images with various interval sizes among accumulators in HT parameter domain

Interval sizes	25	26	27	28	29	30
Failure number	60	21	3	0	22	60
Success number	0	39	57	60	39	0
Success rate	0%	65%	95%	100%	63%	0%

11 and 12 show the initial and corresponding reconstructed base-grid and base-checker images with various interval sizes among accumulators in HT parameter domains, respectively. Tables 1 and 2 indicate the corresponding success rates of the reconstructed base-grid and base-checker images with various interval sizes among accumulators. With selected interval sizes of 37 and 28 among accumulators for the grids pattern and checkers pattern in HT domains, we have the highest success rates of the reconstructed base-grid and base-checker images, respectively. The other interval sizes cause the reconstructed images without containing the whole base elements. The complete reconstructed base element images will be the standard pattern images for comparing with the binary testing images to identify transmitted deformation flaws and locate the flaw positions.

4.2. **Detection results of using two standard patterns with different numbers of line segments and line widths.** How many horizontal and vertical line segments are suitable for a standard pattern to project the line segments on testing images through the transmission of transpicuous glass? In theory, the more line segments in a standard pattern are used, the more precise to present the deformation levels in a testing image. If we change the standard patterns with various numbers of line segments, the detection results of deformation flaws will be different. We examine the grids patterns with three different numbers of line segments, 6, 7, and 8, to quantify the deformation levels of testing images. Figure 13 shows the initial, processed, and resulting images by the proposed method using the grids patterns with the three numbers of line segments. With the selected line segments of 7 and 8 used in the proposed method, more detailed deformation flaws are identified on the testing images. Table 3 indicates the comparisons of performance indices and the detection result using the standard pattern with 7 line segments has better deformation inspection performance because of higher detection rate and middle fake alert rate.

The pixel size of line width in the reconstructed base element image also will affect the detection performance of deformation flaws by the proposed method. If a suitable pixel size of line width is selected in the reconstructed base element image, the smaller deformation flaws will be more completely identified. We examine the grids patterns with 3, 4, and 5 pixel widths and the checkers patterns with 1, 2, and 3 pixel widths of lines in the reconstructed base element images by the proposed method. Figures 14 and 15 show the initial, processed, and resulting images by the proposed method using the grids patterns and the checkers patterns with the three pixel widths, respectively. We find

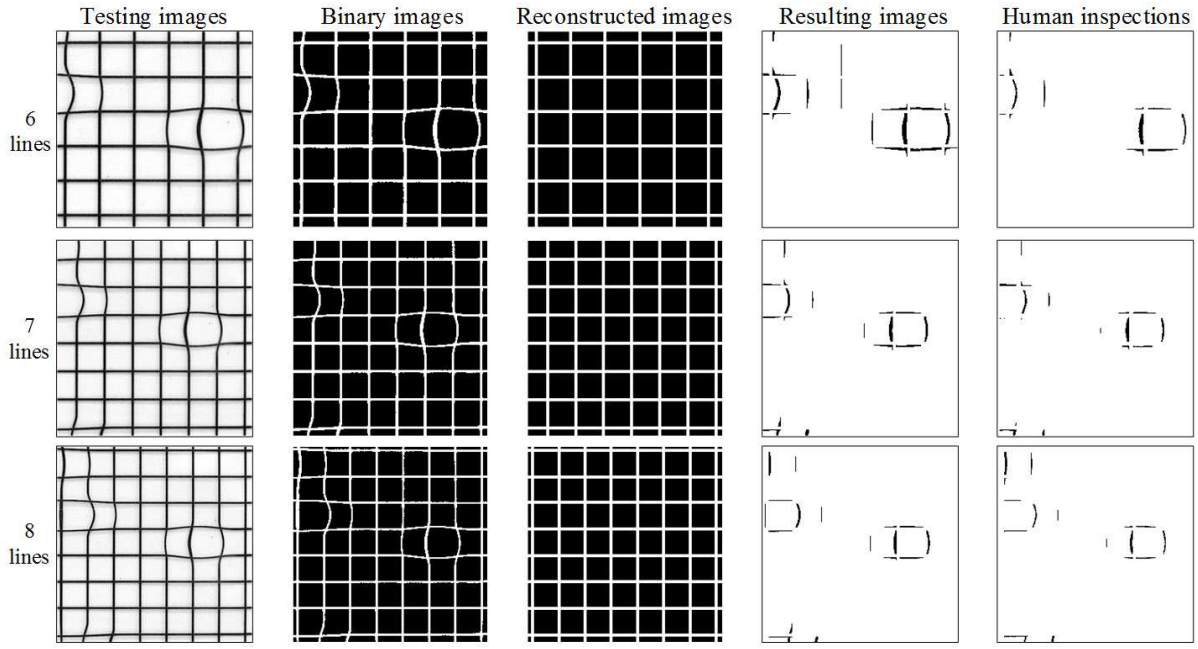

FIGURE 13. Partial results of transmitted deformation inspection by the proposed method for testing images using grids patterns with various numbers of line segments

TABLE 3. Performance indices of transmitted deformation inspection by the proposed method for testing images using grids patterns with various numbers of line segments

	6 lines	7 lines	8 lines
Fake alert rate (α)	1.172%	0.526%	0.390%
Detection rate ($1-\beta$)	79.07%	83.92%	81.55%

that the smaller pixel widths are more sensitive to the detection of deformation flaws and cause more fake alert errors. Tables 4 and 5 indicate the detection results using the 4-pixel width for the grids pattern and 2-pixel width for the checkers pattern are suitable and have better deformation inspection performance because of higher detection rate and middle fake alert rate.

4.3. **Performance assessment of different deformation flaw detection techniques.** Three common standard patterns are used to detect deformation by the proposed approach for differentiating outcomes of deformation flaw inspection. To reveal the deformation inspection effects of original captured images, Figure 16 illustrates partial results of inspecting deformation flaws by the proposed approach using the lines pattern, grids pattern, and checkers pattern, and the gold standard (ground truth) supplied by empirical evaluators, separately. The method using the lines pattern produces some incorrect discernments in losing alerts and the method using the checkers pattern causes several of incorrect discernments in fake alerts on deformation flaw inspection. The proposed method using the grids pattern inspects most of the deformation flaws and produces less incorrect discernments. Consequently, the proposed method with grids pattern is superior to the methods using lines pattern and checkers pattern in the deformation flaw inspection of transpicuous glass images.

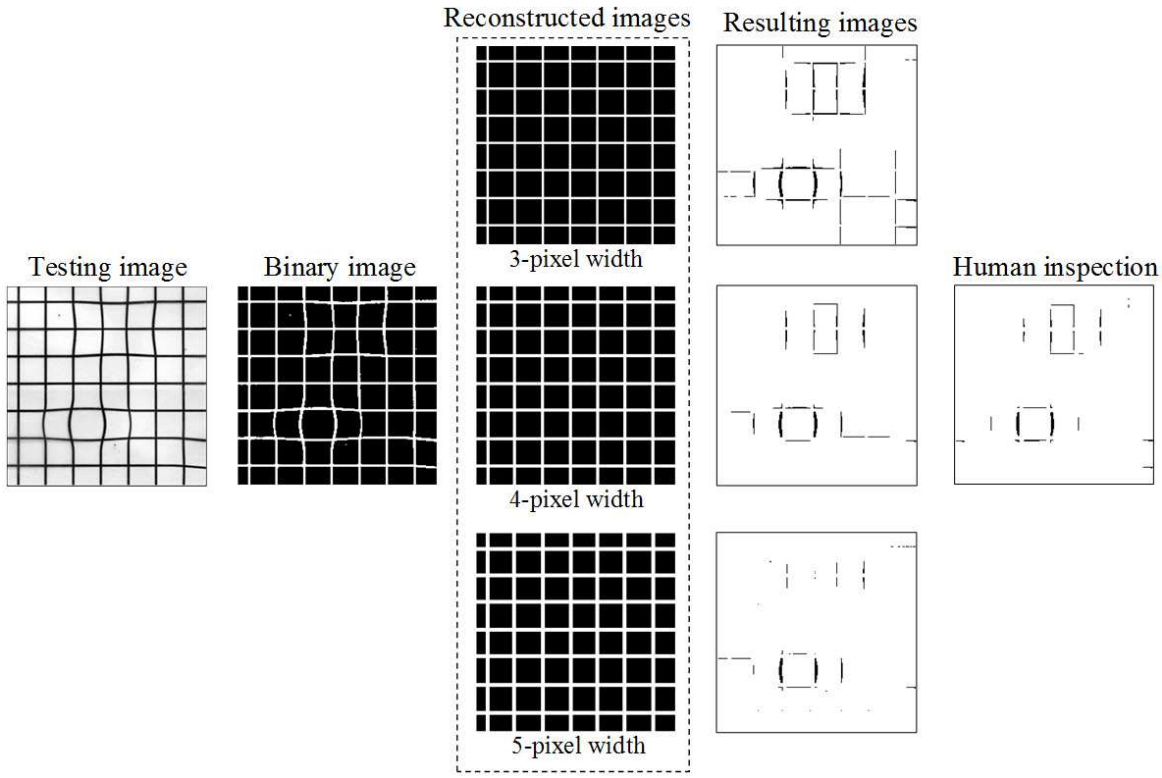

FIGURE 14. Partial results of transmitted deformation inspection by the proposed method for producing reconstructed base-grid images with various line widths

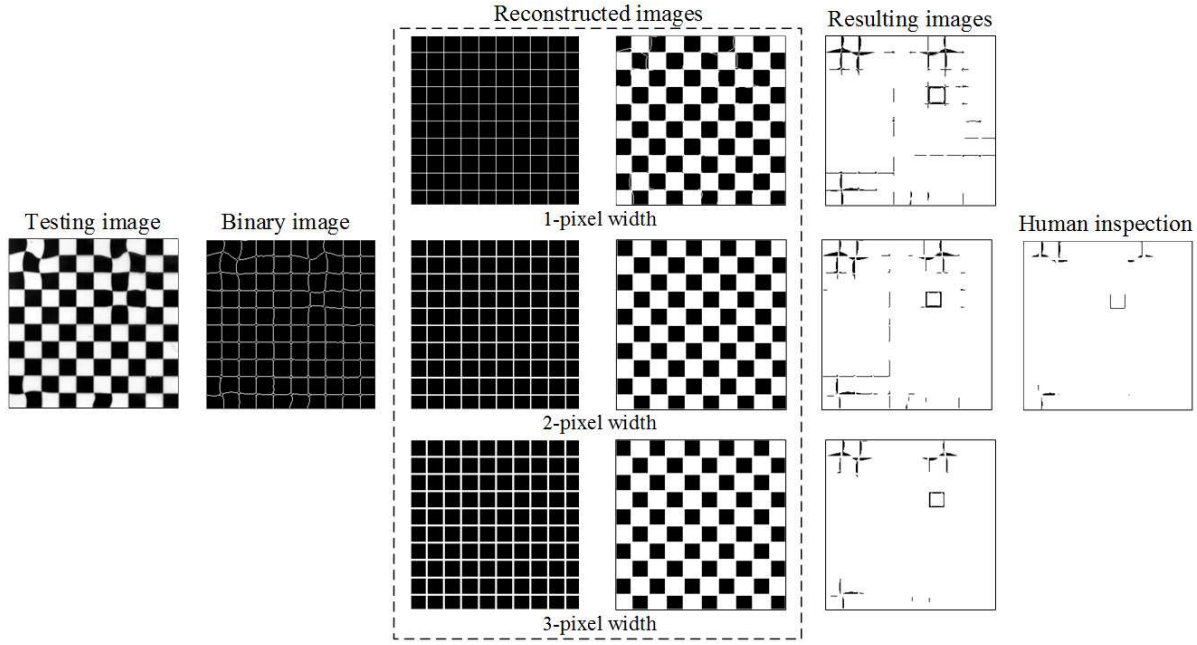

FIGURE 15. Partial results of transmitted deformation inspection by the proposed method for producing reconstructed base-checker images with various line widths

TABLE 4. Performance indices of transmitted deformation inspection by the proposed method for producing reconstructed base-grid images with various line widths

	3-pixel width	4-pixel width	5-pixel width
Fake alert rate (α)	1.951%	0.545%	0.302%
Detection rate ($1-\beta$)	87.3%	83.02%	59.64%

TABLE 5. Performance indices of transmitted deformation inspection by the proposed method for producing reconstructed base-checker images with various line widths

	1-pixel width	2-pixel width	3-pixel width
Fake alert rate (α)	3.308%	2.568%	1.661%
Detection rate ($1-\beta$)	60.24%	75.69%	64.41%

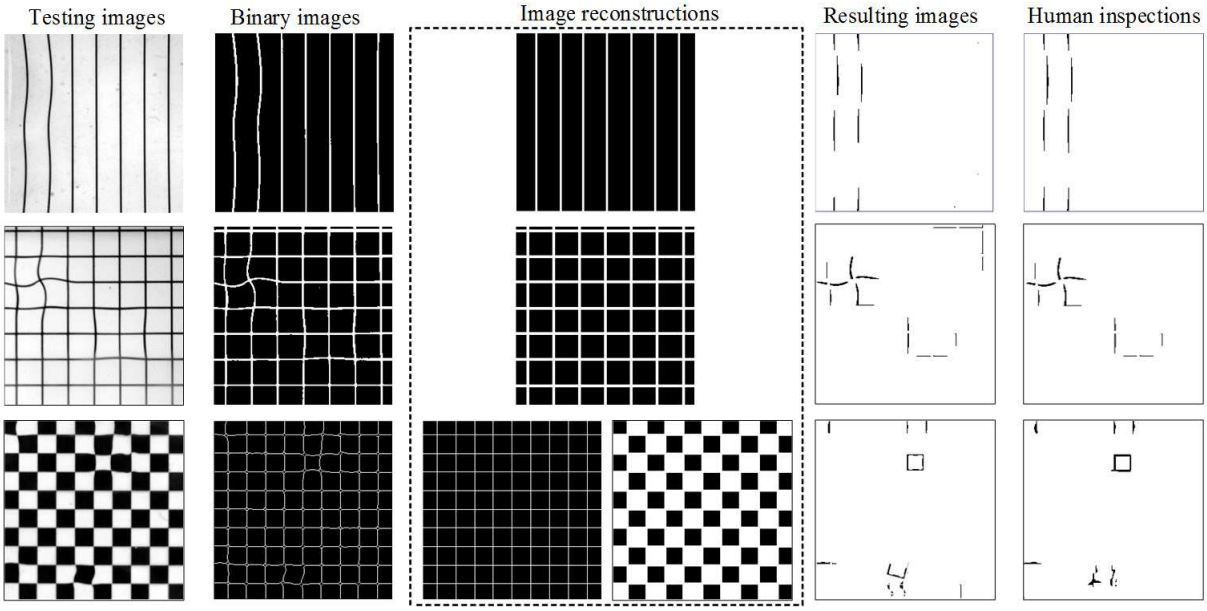

FIGURE 16. Partial results of transmitted deformation inspection by the proposed method using three common standard patterns

TABLE 6. Performance indices of transmitted deformation inspection by the proposed method using three common standard patterns and the Lin and Hsieh method

Standard patterns	Lines pattern	Grids pattern	Checkers pattern	Lin and Hsieh [23]
Detection rate ($1-\beta$)	67.58%	83.85%	75.69%	71.26%
Fake alert rate (α)	0.266%	0.468%	2.568%	0.392%
Processing time (sec.)	0.0845	0.1122	0.4972	0.1486

Table 6 evidences the differentiating outcomes of deformation flaw inspection effects in the conducted experiments. The suggested methods individually using three common standard patterns and the Lin and Hsieh method [23] are evaluated contrary to the results by empirical evaluators. The average deformation detection rates ($1-\beta$) of entire testing

samples by using the three standard patterns are 67.58% by using line pattern, 83.85% by using grids pattern, 75.69% by using checkers pattern, and 71.26% by the Lin and Hsieh method. Nevertheless, the proposed method with checkers pattern has a remarkably greater fake alert rate 2.568%, and the scheme with grids pattern has a rather smaller fake alert rate 0.468%. More specifically, the suggested method with grids pattern has a greater deformation detection rate and possesses a smaller fake alert rate employed to transmitted deformation inspection of transpicuous glass images. The mean processing times for dealing with a captured image having 256×256 pixels are as follows: 0.0845 seconds by using lines pattern, 0.1122 seconds by using grids pattern, 0.4972 seconds by using checkers pattern, and 0.1486 seconds by the Lin and Hsieh method. The average conducting time of the recommended method with checkers pattern is practically four times longer than that of the method with grids pattern. The suggested approach using the grids pattern overcomes the difficulties of inspecting deformation flaws on transpicuous glass images with transmitted and reflected exteriors as well as excels in its capability of accurately discerning deformation flaws from regular regions. Furthermore, through self contrasting the binary testing image and the binary reconstructed image from HT voting procedure, the proposed method is better than the Lin and Hsieh method since it does not require any template for pattern accordance check and there is no need for precise positioning of testing glass products in fixtures.

5. **Conclusions.** This study attempts to find a way to substitute the human evaluators in fabrication process by developing a frequency reconstruction technique established on HT to examine deformation flaws on clear glass products. This research recommends a base element reconstruction approach by HT voting scheme to the visual inspection of deformation flaws on high transmitted appearances of glass images. Experimental outcomes present the proposed method achieves a high 83.85% probability of exactly discriminating deformation flaws and a low 0.468% probability of incorrectly investigating regular districts as deformation flaws on transmitted appearances of transpicuous glass. The suggested method effectively and efficiently prevails over the troubles of inspecting slight deformation flaws on vehicle glass with high transmitted exteriors. Primary limitations of the proposed approach need to be conquered as follows, the method will often fail to detect deformation flaws if they are congregating in narrow neighborhoods of edges, and the method is not sufficiently sensitive to differentiate the deformation flaws with slow variabilities in the deformed shapes. Therefore, further study directions can focus on increasing the sensitivity of detecting the deformation flaws and assessing current techniques to seek for the highly efficient and effective approach for the raised application.

Acknowledgment. This research received the financial support through the Grant MOST 104-2221-E-324-010 provided by the Ministry of Science and Technology, Taiwan.

REFERENCES

[1] A. S. Hassanein, S. Mohammad, M. Sameer and M. E. Ragab, A survey on Hough transform, theory, techniques and applications, *International Journal of Computer Science Issues*, vol.12, issue 1, no.2, pp.139-156, 2015.

[2] A. M. Abu Ebayyeh and A. Mousavi, A review and analysis of automatic optical inspection and quality monitoring methods in electronic industry, *IEEE Access*, vol.8, pp.183192-183271, 2020.

[3] Q. Luo, X. Fang, L. Liu, C. Yang and Y. Sun, Automated visual defect detection for flat steel surface: A survey, *IEEE Trans. Instrumentation and Measurement*, vol.69, no.3, pp.626-644, 2020.

[4] Q. Luo, X. Fang, J. Su, J. Zhou, B. Zhou, C. Yang, L. Liu, W. Gui and L. Tian, Automated visual defect classification for flat steel surface: A survey, *IEEE Trans. Instrumentation and Measurement*, vol.69, no.12, pp.9329-9349, 2020.

[5] Y.-S. P. Chiu, H.-D. Lin and H.-H. Cheng, Optical inspection of appearance faults for auto mirrors using Fourier filtering and convex hull arithmetic, *Journal of Applied Research and Technology*, vol.19, no.4, pp.279-293, 2021.
[6] M. Aslam, T. M. Khan, S. S. Naqvi, G. Holmes and R. Naffa, On the application of automated machine vision for leather defect inspection and grading: A survey, *IEEE Access*, vol.7, pp.176065-176086, 2019.
[7] W.-C. Wang, S.-L. Chen, L.-B. Chen and W.-J. Chang, A machine vision based automatic optical inspection system for measuring drilling quality of printed circuit boards, *IEEE Access*, vol.5, pp.10817-10833, 2017.
[8] B. Zhao, M. Dai, P. Li and X. Ma, Defect detection method for electric multiple units key components based on deep learning, *IEEE Access*, vol.8, pp.136808-136818, 2020.
[9] Y. Qiu, L. Tang, B. Li, S. Niu and T. Niu, Uneven illumination surface defects inspection based on saliency detection and intrinsic image decomposition, *IEEE Access*, vol.8, pp.190663-190676, 2020.
[10] C. Iglesias, J. Martínez and J. Taboada, Automated vision system for quality inspection of slate slabs, *Computers in Industry*, vol.99, pp.119-129, 2018.
[11] G. Fu, P. Sun, W. Zhu, J. Yang, Y. Cao, M. Y. Yang and Y. Cao, A deep-learning-based approach for fast and robust steel surface defects, *Optics and Lasers in Engineering*, vol.121, pp.397-405, 2019.
[12] Y. Shin, M. Kim, K.-W. Pak and D. Kim, Practical methods of image data preprocessing for enhancing the performance of deep learning based road crack detection, *ICIC Express Letters, Part B: Applications*, vol.11, no.4, pp.373-379, 2020.
[13] D. Jeon, U. Jung, K. Park, P. Kim, S. Han, H. Jeong, R. E. Wijesinghe, N. K. Ravichandran, J. Lee, Y. Han, M. Jeon and J. Kim, Vision-inspection-synchronized dual optical coherence tomography for high-resolution real-time multidimensional defect tracking in optical thin film industry, *IEEE Access*, vol.8, pp.190700-190709, 2020.
[14] Q. Zhou, R. Chen, B. Huang, C. Liu, J. Yu and X. Yu, An automatic surface defect inspection system for automobiles using machine vision methods, *Sensors*, vol.19, no.3, DOI: 10.3390/s19030644, 2019.
[15] H.-D. Lin and H.-H. Tsai, Automated quality inspection of surface defects on touch panels, *Journal of the Chinese Institute of Industrial Engineers*, vol.29, no.5, pp.291-302, 2012.
[16] Y.-S. P. Chiu and H.-D. Lin, An innovative blemish detection system for curved LED lenses, *Expert Systems with Applications*, vol.40, no.2, pp.471-479, 2013.
[17] C.-F. J. Kuo, W.-C. Lo, Y.-R. Huang, H.-Y. Tsai, C.-L. Lee and H.-C. Wu, Automated defect inspection system for CMOS image sensor with micro multi-layer non-spherical lens module, *Journal of Manufacturing Systems*, vol.45, pp.248-259, 2017.
[18] C. Mantel, F. Villebro, H. R. Parikh, S. Spataru, G. A. dos Reis Benatto, D. Sera, P. B. Poulsen and S. Forchhammer, Method for estimation and correction of perspective distortion of electroluminescence images of photovoltaic panels, *IEEE Journal of Photovoltaics*, vol.10, no.6, pp.1797-1802, 2020.
[19] F. Cutolo, U. Fontana, N. Cattari and V. Ferrari, Off-line camera-based calibration for optical see-through head-mounted displays, *Applied Sciences*, vol.10, no.1, DOI: 10.3390/app10010193, 2020.
[20] K. M. Gerton, B. J. Novar, W. Brockmeier and C. Putnam, A novel method for optical distortion quantification, *Optometry and Vision Science*, vol.96, no.2, 2018.
[21] R. C. Youngquist, M. Skow and M. A. Nurge, Optical distortion evaluation in large area windows using interferometry, *The 14th International Symposium on Nondestructive Characterization of Materials*, Marina Del Rey, CA, USA, 2015.
[22] M. Dixon, R. Glaubius, P. Freeman, R. Pless, M. P. Gleason, M. M. Thomas and W. Smart, Measuring optical distortion in aircraft transparencies: A fully automated system for quantitative evaluation, *Machine Vision and Applications*, vol.22, no.5, pp.791-804, 2011.
[23] H.-D. Lin and K.-S. Hsieh, Detection of surface variations on curved mirrors of vehicles using slight deviation control techniques, *International Journal of Innovative Computing, Information and Control*, vol.14, no.4, pp.1407-1421, 2018.
[24] P. V. C. Hough, *Method and Means for Recognizing Complex Patterns*, US Patent 3,069,654, Ser. No. 17,7156 Claims, 1962.
[25] R. O. Duda and P. E. Hart, Use of the Hough transformation to detect lines and curves in pictures, *Communications of the ACM*, vol.15, no.1, pp.11-15, 1971.
[26] P. Mukhopadhyay and B. B. Chaudhuri, A survey of Hough transform, *Pattern Recognition*, vol.48, pp.993-1010, 2015.
[27] W.-C. Li and D.-M. Tsai, Defect inspection in low-contrast LCD images using Hough transform-based nonstationary line detection, *IEEE Trans. Industrial Informatics*, vol.7, no.1, pp.136-147, 2011.

[28] C. Ajmi, S. E. Ferchichi, A. Zaafouri and K. Laabidi, Automatic detection of weld defects based on Hough transform, *2019 International Conference on Signal, Control and Communication*, pp.1-6, DOI: 10.1109/SCC47175.2019.9116162, 2019.
[29] Q. Ge, M. Fang and J. Xu, Defect detection of industrial products based on improved Hough transform, *2018 IEEE International Conference on Mechatronics and Automation*, pp.832-836, DOI: 10.1109/ICMA.2018.8484328, 2018.
[30] J. Wang, P. Fu and R. X. Gao, Machine vision intelligence for product defect inspection based on deep learning and Hough transform, *Journal of Manufacturing Systems*, vol.51, pp.52-60, 2019.
[31] Y.-J. Cha, K. You and W. Choi, Vision-based detection of loosened bolts using the Hough transform and support vector machines, *Automation in Construction*, vol.71, pp.181-188, 2016.
[32] R. C. Gonzalez and R. E. Woods, *Digital Image Processing (4 Edition)*, Pearson Education, Harlow, Essex, England, 2018.
[33] J. Canny, A computational approach to edge detection, *IEEE Trans. Pattern Analysis and Machine Intelligence*, vol.8, no.6, pp.679-698, 1986.
[34] N. Otsu, A threshold selection method from gray level histogram, *IEEE Trans. Systems, Man and Cybernetics*, vol.9, pp.62-66, 1979.

Author Biography

Hong-Dar Lin is currently a professor in the Department of Industrial Engineering and Management at Chaoyang University of Technology, Taiwan. He received his Ph.D. degree in industrial engineering from the University of Missouri-Columbia, USA in 1994. His research interests are in quality management, applications of machine vision systems, automated inspection and metrology, machine learning, patterns recognition, and algorithms of information fusion.

Yuan-Chin Lo received the B.Sc. and M.Sc. degrees in Department of Industrial Engineering and Management from Chaoyang University of Technology, Taiwan, 2013 and 2015, respectively. His research interests include quality management, applications of machine vision systems, automated inspection and metrology, and patterns recognition.

Chou-Hsien Lin is currently pursuing the M.Sc. degree in civil engineering at the University of Texas at Austin, USA. He received the B.Sc. degree in architectural engineering from the same institution in 2020. His research interests include indoor air quality, exposure pathways of air pollutants, and the health effects of volatile organic compounds in the built environment.